Catabolite Activator Protein in Aqueous Solution: A Molecular Simulation Study

Marco Berrera,[†,‡,§] Sergio Pantano,[†,‡] and Paolo Carloni*[,†,§]

Scuola Internazionale Superiore di Studi Avanzati (SISSA) and INFM, Democritos Modeling Center for Research In Atomistic Simulation, via Beirut 4, 34014 Trieste, Italy, Venetian Institute of Molecular Medicine (VIMM), via Orus 2, 35129 Padova, Italy, and Istituto Italiano di Tecnologia (IIT), via Beirut 4, 34014 Trieste, Italy

Received: October 16, 2006; In Final Form: December 6, 2006

The homodimeric catabolite activator protein (CAP) is a bacterial DNA binding transcription regulator whose activity is controlled by the binding of the intracellular mediator cyclic adenosine monophosphate (cAMP). Each CAP subunit consists of a cyclic nucleotide and a DNA binding domain. Here, we investigate the structural features of the ligand-bound CAP in aqueous solution by molecular dynamics simulations based on the available X-ray structures (Passner et al. *J. Mol. Biol.* **2000**, *304*, 847−859 and Chen et al. *J. Mol. Biol.* **2001**, *314*, 63−74). Our calculations suggest that the homodimer in solution assumes a symmetric arrangement in which both DNA binding domains are separated from the respective cyclic nucleotide binding domains by a cleft. This contrasts with the X-ray structure, which exhibits instead an asymmetric conformation. On the basis of electrostatics calculations, we propose that the symmetric structure in solution may be an important feature for DNA molecular recognition.

Introduction

The catabolite activator protein (CAP, also called cAMP receptor protein) is a bacterial DNA binding protein involved in the activation of the transcription of several operons.[1−3] Cyclic adenosine monophosphate (cAMP) binding to CAP causes a cascade of structural rearrangements that allows for selective binding to DNA (consensus sequence is 5′-AAATGTGATCT-3′).[4−6] This in turn induces DNA bending[7−11] and a rearrangement of CAP,[12,13] which is followed by the binding of the RNA polymerase enzyme.[14−16]

The X-ray structures of DNA-bound and DNA-free states of CAP have provided key insights into the molecular basis of DNA binding.[7,17−19] These studies have shown that CAP is a homodimer whose subunits (namely, "A" and "B", Figure 1) consist of two domains each. The first domain is the conserved signaling module N-terminal cyclic nucleotide binding domain (CNBD, residues 1−137),[20] which includes an eight-stranded β-roll flanked by an α-helix (A-helix) at its N-term and by two helices (B- and C-helices) at its C-term. A hinge region, which is close to the homodimeric symmetry axis (residues 133−142), connects the CNBD to the C-terminal DNA binding domain (DBD, residues 138−209). The latter includes a helix−turn−helix motif that binds to DNA, inducing a final bend of ∼90°.[7] Two cAMP binding sites for each subunit are present. The primary binding site, which has a micromolar affinity for cAMP,[21,22] is located in the CNBD, within the β-roll, and it is lined by the C-helices of both subunits: binding of cAMP (in its anti conformation) triggers a reorientation of the β4/β5 loops and of the C-helices, which leads to an allosteric change of the hinges that repositions the DBDs and results in DNA binding.[17,20,23−33] Selectivity toward the target DNA sequence is achieved by cAMP binding to the primary sites.[21] The secondary binding site, with millimolar affinity for cAMP, is formed by residues from both domains of the same subunit and from the hinge region of the opposite subunit.[18] DNA binding to CAP depends on cAMP concentration.[21,22,34,35]

In the crystal phase, the structures of the subunits have been found to depend on the state of the protein. In the DNA-bound state, the DBDs are symmetrically arranged and are both packed against their CNBDs (closed conformation for both subunits, Figure 1a).[7,18,19] In the DNA-free X-ray structure, one subunit is in the closed conformation, while the other is separated from its corresponding CNBD by a cleft (open conformation, Figure 1c).[17] It is well-known that crystal packing forces may induce structural modifications in proteins.[36,37] Therefore, the structure of such subunits in aqueous solution might differ significantly from that in the crystal. As shown in Figure 1b, in the X-ray structure, several DBD residues exhibit close contacts with other proteins. Therefore, the crystal packing is potentially responsible for possible deviations from the biologically relevant protein conformation. Here, we address this issue by undertaking a comparative molecular dynamics (MD) study of the protein in the crystal phase and in aqueous solution.

Our MD calculations of the crystal turn out to reproduce the structure of the protein experimentally observed (in particular the closed−open conformation, Figure 1c), suggesting that our computational setup provides a relatively accurate description of the system. In addition, the ligand-bound protein in solution assumes an open−open symmetric conformation (Figure 1d). Such a conformation could play a key role in DNA molecular recognition.

Methods

The following models are constructed: (i) CAP_{cryst} is the X-ray structure from *Escherichia coli* solved at a resolution of 2.10 Å (pdb entry code 1G6N,[17] Figure 1b); (ii) CAP_{aq} is based on the same X-ray structure,[17] although only one asymmetric unit is considered (Figure 1c); (iii) CAP^{*}_{aq} is the protein in

* To whom correspondence should be addressed. E-mail: carloni@sissa.it.
† SISSA and INFM.
‡ VIMM.
§ IIT.

10.1021/jp0667893 CCC: $37.00
Published on Web 01/23/2007

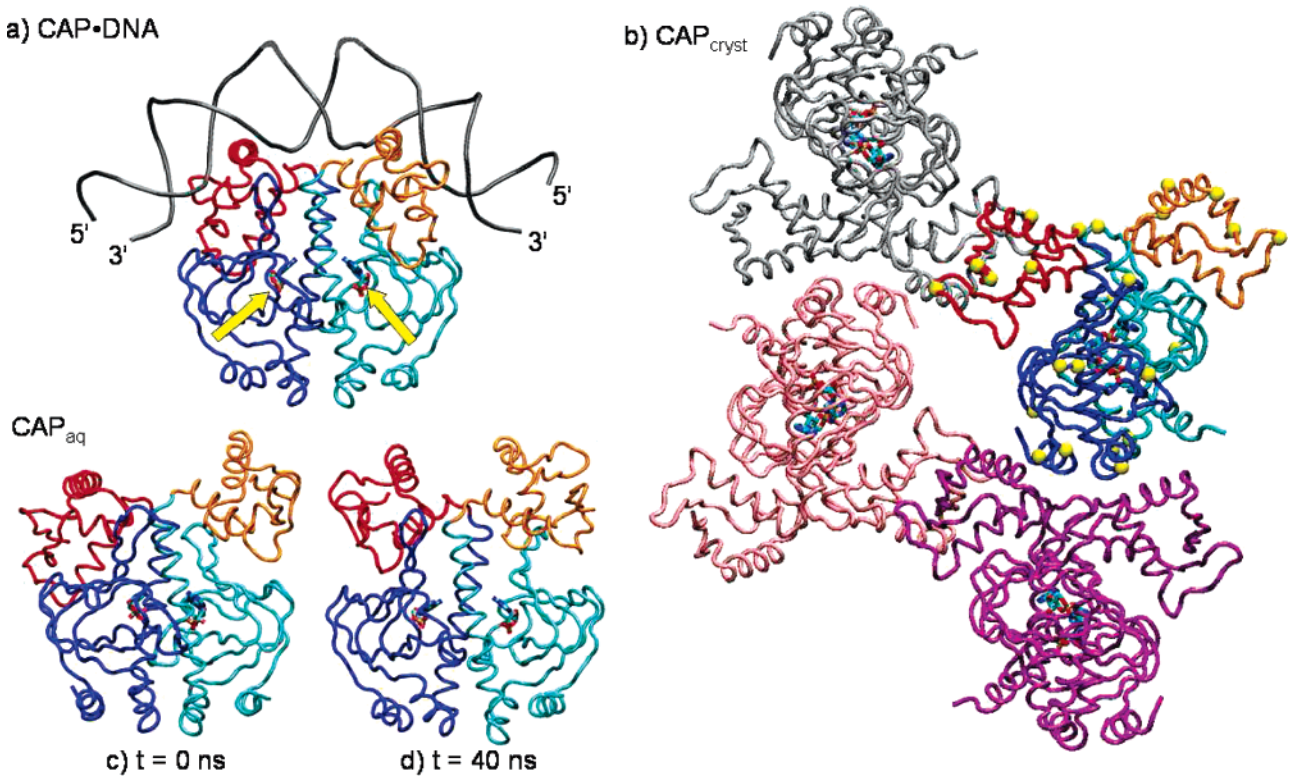

Figure 1. Structures of CAP: (a) The asymmetric unit of the DNA-bound CAP X-ray structure (CAP•DNA),[18] (b) the unit cell of the DNA-free CAP in the crystal lattice (CAP$_{cryst}$)[17] and CAP in aqueous solution (CAP$_{aq}$) in the initial (c) and in the final (d) MD conformations are reported as ribbons. Water molecules are omitted for clarity. The CNBD and the DBD of subunit A are colored in blue and red, respectively, while the same domains of subunit B are colored in cyan and orange, respectively; the cAMP molecules are drawn in sticks and colored by the atom type; only in part a, the cAMP binding sites are indicated by the yellow arrows and DNA (sequence 5′-GCGAAAAATGCGATCTAGATCGCATTTTTCG-3′) is represented as a gray double strand. In CAP$_{cryst}$, one asymmetric unit, which is rotated with respect to the other panels, is colored as above and the yellow spheres indicate the residues forming crystal packing contacts (interresidue distance between non-hydrogen atoms smaller than 0.35 nm); the remaining three protein molecules in the unit cell are shown in different colors. The graphics were obtained with the VMD program.[69]

TABLE 1: Selected Features from the MD Calculations[a]

complex name	based on	*a* (nm)	*b* (nm)	*c* (nm)	no. of amino acids	no. of cAMP molecules	no. of water molecules	no. of Na^+ ions
CAP$_{aq}$	1G6N[17]	7.40	9.15	8.52	401	2	16 954	2
CAP$^*_{aq}$	1O3T[18]	8.99	7.05	9.09	396	2	16 995	0
CAP$_{cryst}$	1G6N[17]	4.68 (<0.01)	9.55 (−0.01)	10.54 (−0.01)	1604	8	8000	8

[a] The table shows the pdb entry codes of the initial X-ray structures, the mean dimensions of the MD unit cell after equilibration, and the number of amino acids, cAMP molecules, water molecules, and sodium ions, which are added to neutralize the box. In CAP$_{cryst}$, the differences between the calculated and experimental values of the cell parameters are reported in parentheses.

aqueous solution obtained by removing the DNA from the X-ray structure of the CAP−DNA complex from *Escherichia coli* solved at a resolution of 2.80 Å (pdb entry code 1O3T,[18] Figure 1a and Supporting Information Figure 2). In all systems, one cAMP molecule is bound to both CNBDs, acidic and basic residues are assumed to be ionized under the physiological conditions, and hydrogens are added by assuming standard bond lengths and angles. Sodium ions are added to achieve neutrality (Table 1).

Solvation. CAP$_{aq}$ and CAP$^*_{aq}$ are solvated by adding a water model with 1.0 kg/L density into the parallelepiped simulation boxes that contain the different solutes. Solvent molecules are rejected if the distance between any solvent atom and the closest solute atom is lower than the sum of their respective van der Waals radii. This procedure generates around the solute small voids that are filled after a short solvent simulation in the NPT ensemble (i.e., 60 ps of MD using the Berendsen thermostat and barostat[38] with $T = 300$ K, $P = 1$ atm, and 1 ps time constants) with a reduction of the MD box volume. The protein in the crystal lattice solvated using the procedure described above shows several cavities which could be filled by water.[39] Thus, a different solvation procedure is used for CAP$_{cryst}$. We define a grid of ∼0.29 nm size spanning the entire unit cell, and water oxygens are placed at any grid point if the corresponding grid cell is empty, that is, if no solute atom is found in the given cell. The solvent equilibration dynamics (60 ps) is sufficient to restore the normal water structure, as confirmed by a comparison with the crystal solvated with the standard procedure outlined above (data not shown).

Molecular Dynamics. We use the AMBER94 force field[40,41] for protein, DNA, and ions and the TIP3P force field[42] for water. The force field for cAMP is developed in ref 43 and is proven to reliably reproduce the molecule interactions within several cAMP binding proteins.[43−45]

Rectangular periodic boundary conditions are applied to each system. For the CAP$_{cryst}$ system, the four homodimers present in the crystallographic unit cell are explicitly considered in the simulation box, whose dimensions are identical to the experimental unit cell parameters. Thus, periodic boundary conditions reproduce the experimental orthorhombic lattice, mimicking the

crystal-like environment. For the other MD systems, only one CAP homodimer is considered and the box dimensions are large enough to ensure that the minimum distance between the periodic images of the complexes in solution is considerably larger than in the former case. This setup allows for large conformational changes and mimicks solution-like conditions (Table 1). The particle mesh Ewald method is used to evaluate long range electrostatics,[46−48] with a grid spacing smaller than 0.1 nm and 10^{-5} tolerance. A cutoff of 1 nm is used for the real part of the electrostatic interactions and for the van der Waals interactions. The minimum distances between the periodic images of the complexes in solution turn out to always be greater than the short range interactions cutoff. Constraints are applied to all chemical bonds using the LINCS algorithm.[49] The integration time step is set to 1.5 fs.

After an energy minimization and 60 ps of solvent simulation, using the Berendsen thermostat and barostat[38] ($T = 300$ K and $P = 1$ atm), molecular dynamics (MD) simulations are performed in the NPT ensemble, using the Nosé−Hoover thermostat[50,51] and the Parrinello−Rahman procedure[52,53] ($T = 300$ K and $P = 1$ atm); the pressure coupling is isotropic. The temperature and pressure time constants are set to 1 ps. CAP_{aq}, CAP^{*}_{aq}, and CAP_{cryst} are simulated for 40, 15, and 15 ns of MD, respectively. The calculations are performed using the GROMACS program.[54,55]

Snapshots collected every 15 ps are analyzed to obtain the following properties: (i) Root-mean-square deviations (rmsd's) of the Cα atoms are calculated after least-squares fit to the respective X-ray structure,[17,18] if not otherwise specified. (ii) The contact surface between the asymmetric units in the crystal phase is estimated as the difference between the solvent accessible surface areas[56] calculated for each homodimer alone and in the crystal complex.[57] (iii) Essential mode (EM) analysis of the Cα atoms is used to identify large collective motions.[58−62]

Electrostatics. The Poisson−Boltzmann equation[63,64] is used to calculate the electrostatic potential at and outside of the protein surface, using the APBS program;[65] a two-run focusing procedure is applied with a 0.06 nm final grid spacing; a 100 mM monovalent ionic concentration, 300 K temperature, protein dielectric constant of $\epsilon_{in} = 1$, and solvent dielectric constant of $\epsilon_{wat} = 80$ are assumed. The calculations are carried out for the protein in the initial conformation in the CAP^{*}_{aq} MD system as well as for the structure after 40 ns of MD in the CAP_{aq} MD system (closed and open conformations, respectively).

Results and Discussion

CAP_{cryst}. In the X-ray structure of the DNA-free cAMP-bound CAP,[17] the unit cell contains four asymmetric units, each consisting of a protein homodimer. Several crystal packing contacts, that is, contacts between residues from different asymmetric units, are observed. They comprise residues spread throughout the protein structure (Table 2 and Figure 1b), in particular Arg-169, Arg-180, and Arg-185, which are involved in protein−DNA interactions. Here, we perform 15 ns of MD simulation of the protein under the crystal-like conditions, to check whether our computational setup (see Methods) is able to reproduce the determinants of the X-ray structure.

The residues forming crystal packing contacts maintain the interaction between different homodimers during the simulation, as estimated by an analysis of the distances between couples of residues and by a calculation of the contact surface between different homodimeric proteins. These residues contribute to the contact surface with an area of at least 0.1 nm^2 each (Table 2).

TABLE 2: Crystal Packing Contacts in CAP_{cryst}[17] [a]

	residue		subunit		residue		subunit	minimum distance (nm)
**	GLU	12	A	**	ARG	185	B	0.31 (0.05)
*	HIS	19	A	*	GLU	55	B	0.42 (0.12)
	SER	27	A	**	GLU	37	B	0.35 (0.03)
	THR	28	A	**	GLU	37	B	0.27 (0.01)
	VAL	43	A	**	ARG	185	B	0.44 (0.10)
	GLU	55	A	*	HIS	31	B	0.58 (0.16)
	GLU	81	A	*	HIS	21	B	0.60 (0.15)
**	GLN	104	A	*	ASP	138	A	0.36 (0.08)
	PRO	160	A	*	ARG	180	B	0.51 (0.16)
**	ARG	169	A	**	PRO	160	B	0.40 (0.13)
**	ARG	185	A		GLN	107	B	0.44 (0.12)
**	ARG	185	A		PRO	110	B	0.38 (0.05)
*	GLY	200	A	**	ASN	194	B	0.48 (0.14)
**	LYS	201	A	**	ASN	194	B	0.34 (0.06)
**	LYS	201	A	*	TYR	206	B	0.39 (0.09)

[a] Contacts are defined for couples of residues from different asymmetric units with non-hydrogen atoms closer than 0.35 nm in the initial X-ray structure,[17] and the minimum distance between non-hydrogen atoms is calculated in the CAP_{cryst} MD simulation: the average value and the corresponding standard deviation of these distances throughout the MD trajectory are reported in the last column. Each listed residue forms a mean contact surface with different asymmetric units of at least 0.1 nm^2 in the initial and in the final MD conformations; the residues forming a mean contact surface of at least 0.3 and 0.7 nm^2 are indicated by one and two asterisks, respectively.

To characterize the closed (subunit A, colored in blue and red in Figure 1) and open (subunit B, colored in orange and cyan in Figure 1) states, we monitor the distances between the mass centers of the DBD and CNBD of the same subunit (2.66 and 2.92 nm, respectively, in the initial conformation). The calculated values are 2.61 (0.06) nm and 2.98 (0.05) nm (Figure 2d), in good accord with the experimental data. The rmsd's of the unit cell and for the four homodimers are 0.16 (0.03) nm and 0.13 (0.02) nm, respectively (Figure 2a). Finally, our calculations turn out to reproduce the experimental unit cell parameters within 0.01 nm (Table 1).[66] We conclude that our calculations are able to reproduce the X-ray structure.

CAP_{aq}. We now relax the CAP structure in aqueous solution. One of the four asymmetric units in the X-ray structure[17] is immersed in a water box consisting of ∼17 000 molecules (Table 1) with two sodium counterions. The system undergoes 40 ns of MD simulation. During the dynamics, the rmsd fluctuates at ∼0.2 nm in the first part of the simulation and increases to ∼0.4 nm after 10 ns (Figure 2b), indicating the presence of a transition. The protein moves to a conformation in which the DBD of subunit A is separated from the respective CNBD by a cleft, as initially observed in subunit B. To filter the large scale concerted structural rearrangements from small harmonic fluctuations, we use essential mode (EM) analysis.[58−62] This method consists of a diagonalization of the covariance matrix of atomic fluctuations. The resulting eigenvectors are ordered with decreasing eigenvalues, which are proportional to the percentage of total fluctuation the corresponding EM describes. Therefore, the eigenvector with the highest eigenvalue describes the collective motion that most accounts for the structural fluctuations. In our case, the conformational transition featured by the DBD of subunit A is described by the first EM, whose eigenvalue accounts for ∼60% of the total motion of the protein, with a cosine content of 0.69.[60−62] Indeed, the projection of this eigenvector on the Cartesian trajectory closely resembles the rmsd trace. It reaches a plateau within 13 ns (Figure 2, inset) and correlates with the increase of the distance between the mass centers of the two domains of subunit A (Figure 2e and animation in ref 67). Then, the protein fluctuates

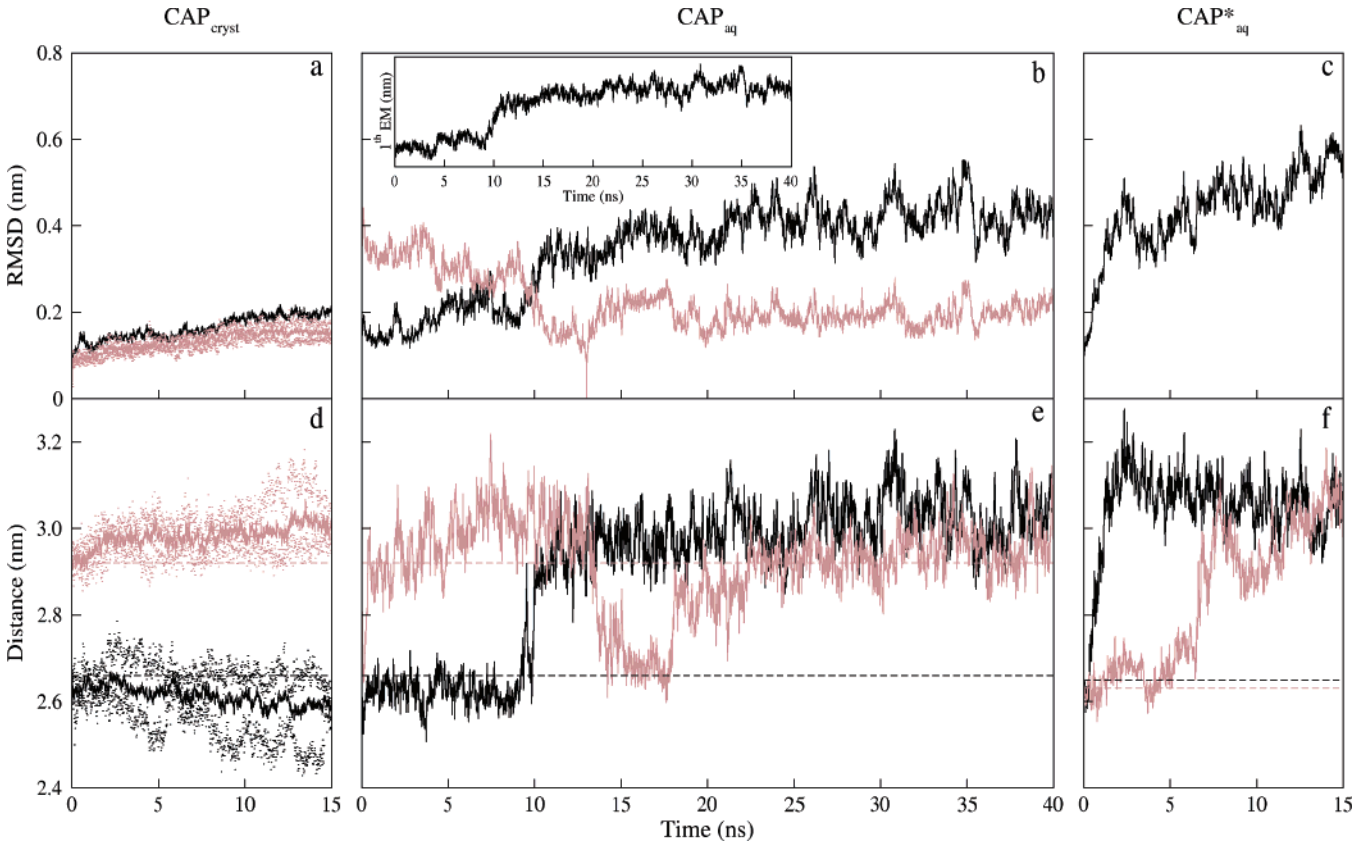

Figure 2. MD simulations: (a−c) rmsd of the CAP_{cryst}, CAP_{aq}, and CAP^{*}_{aq} plotted as a function of the simulation time (black lines). In part a, the rmsd is also averaged over the four protein molecules in the unit cell, considering each molecule separately, and extreme values are reported as dots (mauve line). In part b, rmsd's are also calculated using the structure after 13 ns of MD as the reference conformation (mauve line); the inset shows the principal component of the EM with the highest eigenvalue. (d−f) Distances between the CNBD and DBD mass centers in subunits A and B (solid and mauve lines, respectively) of CAP in the CAP_{cryst}, CAP_{aq}, and CAP^{*}_{aq}, plotted as a function of the simulation time. Initial distances are indicated by the horizontal dashed lines. In part d, distances are averaged over the four asymmetric units of the unit cell and extreme values are indicated by dots.

around the new symmetric open conformation: in fact, in the last 27 ns of MD, the rmsd calculated using the reference structure of the conformation after 13 ns (available in ref 67) is ∼0.2 nm (Figure 2b) and the mean distances between intrasubunit DBD and CNBD mass centers are 3.01 (0.06) nm and 2.89 (0.10) nm for subunits A and B, respectively (Figure 2e). This indicates that the protein fluctuates close to this symmetric open conformation (Figure 1d) within the 27 ns time scale. In addition, the residues that form packing contacts in CAP_{cryst} are more solvent exposed in the CAP_{aq} open conformation than under the crystal conditions, and no new interaction is observed with the rest of the protein.

CAP^{*}_{aq}. In order to check the dependence of our results on the initial model used, we carry out an MD simulation of CAP in aqueous solution based on a different initial conformation, the symmetric closed conformation of CAP that is observed in the X-ray structure of the protein in the complex with DNA[18] (Figure 1a). DNA is not included in our simulation. The rmsd increases and then oscillates around a value of ∼0.5 nm (Figure 2c). Almost at the beginning of the simulation (at ∼1 ns of MD), the DBD of subunit A reorients to the open conformation, and the DBD of subunit B undergoes a similar change within the first 10 ns. After 15 ns of MD, the distances between the mass centers of the DBD and the corresponding CNBD are 3.11 and 3.03 nm for subunits A and B, respectively (Figure 2f). This suggests that the protein in solution moves to the open conformation independently from the initial structure (Supporting Information Figure 2).

In conclusion, our simulations suggest that the DNA-free ligand-bound protein in aqueous solution assumes an open conformation, in which both DBDs are separated from the respective CNBD by a large cleft (Figure 1d). This result holds true independently from two, different, initial structures used in the simulation. Thus, the asymmetry of the experimental X-ray structure, which is reproduced by our computational setup, is possibly caused by packing contacts within the crystal environment (Figure 1b and Table 2). Such an open conformation could play a role in the process of DNA binding.

Electrostatic Profiles. To provide further insights into DNA molecular recognition by CAP, we carry out a comparative electrostatic analysis between the structure of the CAP bound to DNA (closed conformation, Figure 1a) and our model in solution (open conformation, Figure 1d).

When the protein is in the closed conformation, as in the DNA-bound complex[18] (Figure 1a), the DNA binding interface of the protein is characterized by a dominant positive area, which provides an electrostatic complementarity to DNA (Figure 3a,c). On the contrary, the electrostatic potential at the same surface of the protein in the open conformation (calculated here on the CAP_{aq} final MD structure, Figure 1d) appears qualitatively different in the proximity of the homodimeric symmetry axis, that is, near the hinge regions (Figure 3b,d). Since the reorientation of the hinges is a key step in the allosteric mechanism coupling the two domains,[17,23,25] differences in this region might play a role. The charged residues in this region are Asp-138 and Arg-142. In the open conformation, the Arg-142 side chains

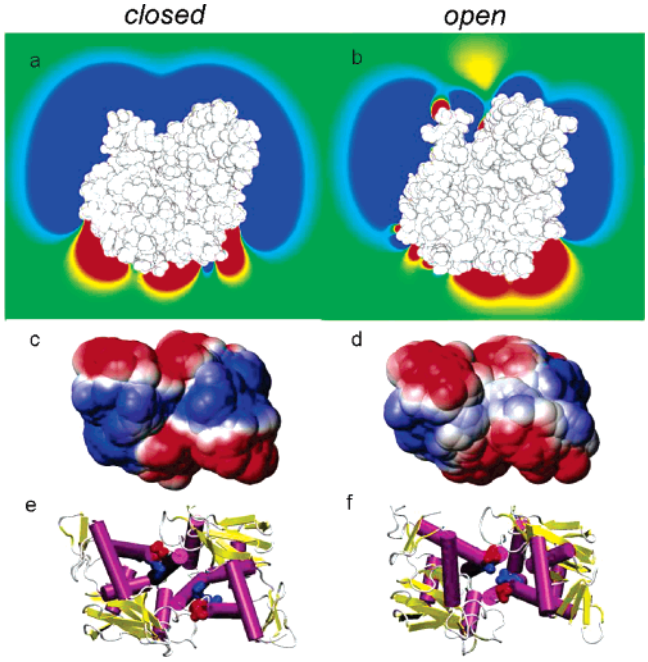

Figure 3. Electrostatic properties: (a and b) van der Waals surface (colored in white) of the protein in the closed (CAP·DNA, a) and open (CAP_{aq} after 40 ns of MD simulation, b) conformations. The molecules are oriented as in Figure 1. The electrostatic potential is plotted on the plane defined by the positions of Cα atoms of Arg-180 from subunits A and B, and by the midpoint between Pro-110 Cα atoms, and is colored in red at −125 mV and in blue at +125 mV. The pictures are obtained using the gOPENMOL program.[70,71] (c−f) View of the protein rotated by 90° relative to parts a and b, which shows the DNA binding interface region. Both the closed (c and e) and open (d and f) states are plotted as a van der Waals surface (c and d) or as a cartoon (e and f). In parts c and d, the electrostatic potential is plotted on the protein surface drawn by the center of a probe of radius 0.5 nm and colored in red at −20 mV and in blue for +20 mV, using the MOLMOL program.[72] In parts e and f, helices are colored in violet and strands in yellow; Asp-138 and Arg-142 are drawn in sticks and colored in red and blue, respectively.

are buried within the intersubunit region (Figure 3f), while, in the closed conformation, they are exposed to the DNA binding interface (Figure 3e). The differences in the electrostatic profiles are also due to Asp-138, which is known to play a crucial role in transmitting the allosteric signal.[25] In fact, the Asp-138 residues are closer to the dimeric symmetry axis of the protein in the open conformation (Figure 3e,f). Thus, when the protein is in the open conformation, the dominant positive potential at the DNA binding interface is intercalated by a negative region in the central part of the surface (Figure 3b,d).

Conclusion

MD simulations are used here to investigate the structural features of the cAMP-activated CAP in solution, providing complementary information that does not emerge from the available X-ray structures.

Our calculations suggest that crystal packing contacts affect the DNA-free CAP conformation and that the ligand-activated form of CAP is the symmetric open conformation (Figure 1d). However, we cannot rule out further conformational rearrangements or fluctuations slower than those that can be sampled by the state-of-the-art MD. Eventual differences between our theoretical results and the actual protein conformation in vivo may be due to the lack in our simulations of the complete biological milieu and to the relatively short time scale that is explored.

The protein structure obtained by our MD simulations in aqueous solution (open conformation, Figure 1d) differs from that of the protein in the DNA-bound X-ray structure (closed conformation, Figure 1a)[7,18,19] not only for the orientation of the DBDs but also for the electrostatic potential at the DNA binding interface. In fact, the latter conformation presents a large positive region, which in the open conformation is interrupted in the proximity of the hinges (Figure 3). We speculate that this electrostatic profile may mediate a first step of DNA bending. Before the molecules get in direct contact, the positive regions of the DNA binding interface of the protein in the open conformation attract the DNA, while a kink is generated in DNA segments prone to bending.[3,68] Subsequently, both macromolecules could attain the direct contact and a mutually induced-fit mechanism could drive the complex from the open to the closed conformation, which provides a larger complementary electrostatic surface for the bound DNA (Figure 3). Further, experimental and/or computational studies are required to test this hypothesis.

Acknowledgment. The authors acknowledge CINECA for computational support. We would like to thank Dr. Aneta Bozena Jezierska for a critical reading of the manuscript.

Supporting Information Available: Discussion of the simulation of CAP with a lower water content than that in CAP_{cryst}, figure showing rmsd plotted as a function of the simulation time and the distances between CNBD and DBD mass centers in subunits A and B plotted as a function of the simulation time, and trace representation of the structure of CAP in aqueous solution in the initial conformation and after 15 ns of MD. This material is available free of charge via the Internet at http://pubs.acs.org.

References and Notes

(1) Kolb, A.; Busby, S.; Buc, H.; Garges, S.; Adhya, S. *Annu. Rev. Biochem.* **1993**, *62*, 749−795.
(2) Busby, S.; Ebright, R. H. *J. Mol. Biol.* **1999**, *293*, 199−213.
(3) Lawson, C. L.; Swigon, D.; Murakami, K. S.; Darst, S. A.; Berman, H. M.; Ebright, R. H. *Curr. Opin. Struct. Biol.* **2004**, *14*, 10−20.
(4) Adhya, S.; Ryu, S.; Garges, S. *Subcell. Biochem.* **1995**, *24*, 303−321.
(5) Harman, J. G. *Biochim. Biophys. Acta* **2001**, *1547*, 1−17.
(6) Berg, O. G.; von Hippel, P. H. *J. Mol. Biol.* **1988**, *200*, 709−723.
(7) Schultz, S. C.; Shields, G. C.; Steitz, T. A. *Science* **1991**, *253*, 1001−1007.
(8) Kahn, J. D.; Crothers, D. M. *Proc. Natl. Acad. Sci. U.S.A.* **1992**, *89*, 6343−6347.
(9) Heyduk, T.; Lee, J. C. *Biochemistry* **1992**, *31*, 5165−5171.
(10) Dixit, S. B.; Andrews, D. Q.; Beveridge, D. L. *Biophys. J.* **2005**, *88*, 3147−3157.
(11) Dixit, S. B.; Beveridge, D. L. *Biophys. J.* **2005**, *88*, L04−L06.
(12) Sogaard-Andersen, L.; Mironov, A. S.; Pedersen, H.; Sukhodelets, W.; Valentin-Hansen, P. *Proc. Natl. Acad. Sci. U.S.A.* **1991**, *88*, 4921−4925.
(13) Baichoo, N.; Heyduk, T. *J. Mol. Biol.* **1999**, *290*, 37−48.
(14) Zhou, Y.; Zhang, X.; Ebright, R. H. *Proc. Natl. Acad. Sci. U.S.A.* **1993**, *90*, 6081−6085.
(15) Jin, R.; Sharif, K. A.; Krakow, J. S. *J. Biol. Chem.* **1995**, *270*, 19213−19216.
(16) Niu, W.; Kim, Y.; Tau, G.; Heyduk, T.; Ebright, R. H. *Cell* **1996**, *87*, 1123−1134.
(17) Passner, J. M.; Schultz, S. C.; Steitz, T. A. *J. Mol. Biol.* **2000**, *304*, 847−859.
(18) Chen, S.; Vojtechovsky, J.; Parkinson, G. N.; Ebright, R. H.; Berman, H. M. *J. Mol. Biol.* **2001**, *314*, 63−74.
(19) Passner, J. M.; Steitz, T. A. *Proc. Natl. Acad. Sci. U.S.A.* **1997**, *94*, 2843−2847.
(20) Berman, H. M.; Ten, Eyck, L. F.; Goodsell, D. S.; Haste, N. M.; Kornev, A.; Taylor, S. S. *Proc. Natl. Acad. Sci. U.S.A.* **2005**, *102*, 45−50.

(21) Scott, S. P.; Jarjous, S. *Biochemistry* **2005**, *44*, 8730−8748.
(22) Chattopadhyay, R.; Parrack, P. *Arch. Biochem. Biophys.* **2006**, *447*, 80−86.
(23) Aiba, H.; Nakamura, T.; Mitani, H.; Mori,; H. *EMBO J.* **1985**, *4*, 3329−3332.
(24) Kim, J.; Adhya, S.; Garges, S. *Proc. Natl. Acad. Sci. U.S.A.* **1992**, *89*, 9700−9704.
(25) Ryu, S.; Kim, J.; Adhya, S.; Garges, S. *Proc. Natl. Acad. Sci. U.S.A.* **1993**, *90*, 75−79.
(26) Baichoo, N.; Heyduk, T. *Biochemistry* **1997**, *36*, 10830−10836.
(27) Krueger, S.; Gorshkova, I.; Brown, J.; Hoskins, J.; McKenney, K. H.; Schwarz, F. P. *J. Biol. Chem.* **1998**, *273*, 20001−20006.
(28) Malecki, J.; Polit, A.; Wasylewski, Z. *J. Biol. Chem.* **2000**, *275*, 8480−8486.
(29) Won, H. S.; Yamazaki, T.; Lee, T. W.; Yoon, M. K.; Park, S. H.; Kyogoku, Y.; Lee, B. J. *Biochemistry* **2000**, *39*, 13953−13962.
(30) Lanzilotta, W. N.; Schuller, D. J.; Thorsteinsson, M. V.; Kerby, R. L.; Roberts, G. P.; Poulos, T. L. *Nat. Struct. Biol.* **2000**, *7*, 876−880.
(31) Chan, M. K. *Nat. Struct. Biol.* **2000**, *7*, 822−824.
(32) Dong, A.; Malecki, J. M.; Lee, L.; Carpenter, J. F.; Lee, J. C. *Biochemistry* **2002**, *41*, 6660−6667.
(33) Youn, H.; Kerby, R. L.; Conrad, M.; Roberts, G. P. *J. Biol. Chem.* **2006**, *281*, 1119−11127.
(34) Heyduk, T.; Lee, J. C. *Biochemistry* **1989**, *28*, 6914−6924.
(35) Heyduk, T.; Lee, J. C. *Proc. Natl. Acad. Sci. U.S.A.* **1990**, *87*, 1744−1748.
(36) van Gunsteren, W. F.; Karplus, M. *Nature* **1981**, *293*, 677−678.
(37) Oakley, A. J.; Loscha, K. V.; Schaeffer, P. M.; Liepinsh, E.; Pintacuda, G.; Wilce, M. C.; Otting, G.; Dixon, N. E. *J. Biol. Chem.* **2005**, *280*, 11495−11504.
(38) Berendsen, H. J. C.; Postma, J. P. M.; DiNola, A.; Haak, J. R. *J. Chem. Phys.* **1984**, *81*, 3684−3690.
(39) Test MD calculation of such a system results in a small shrinking of the cell lattice, although the protein structure is maintained (see the Supporting Information).
(40) Wang, J.; Cieplak, P.; Kollman, P. A. *J. Comput. Chem.* **2000**, *21*, 1049−1074.
(41) Ponder, J. W.; Case, D. A. *Adv. Protein Chem.* **2003**, *66*, 27−85.
(42) Jorgensen, W. L.; Chandrasekhar, J.; Madura, J.; Klein, M. L. *J. Chem. Phys.* **1983**, *79*, 926−935.
(43) Punta, M.; Cavalli, A.; Torre, V.; Carloni, P. *Proteins* **2003**, *52*, 332−338.
(44) Pantano, S.; Zaccolo, M.; Carloni, P. *FEBS Lett.* **2005**, *579*, 2679−2685.
(45) Berrera, M.; Pantano, S.; Carloni, P. *Biophys. J.* **2006**, *90*, 3428−3433.
(46) Darden, T.; York, D.; Pedersen, L. *J. Chem. Phys.* **1993**, *98*, 10089−10092.
(47) Essmann, U.; Perera, L.; Berkowitz, M. L.; Darden, T.; Lee, H.; Pedersen, L. G. *J. Chem. Phys.* **1995**, *103*, 8577−8593.
(48) Sagui, C.; Darden, T. A. *Annu. Rev. Biophys. Biomol. Struct.* **1999**, *28*, 155−179.
(49) Hess, B.; Bekker, H.; Berendsen, H. J. C.; Fraaije, J. G. E. M. *J. Comput. Chem.* **1997**, *18*, 1463−1472.
(50) Nosé, S. *Mol. Phys.* **1984**, *52*, 255−268.
(51) Hoover, W. G. *Phys. Rev. A* **1984**, *31*, 1695−1697.
(52) Parrinello, M.; Rahman, A. *J. Appl. Phys.* **1981**, *52*, 7182−7190.
(53) Nosé, S.; Klein, M. L. *Mol. Phys.* **1983**, *50*, 1055−1076.
(54) Berendsen, H. J. C.; van der Spoel, D.; van Drunen, R. *Comput. Phys. Commun.* **1995**, *91*, 43−56.
(55) Lindahl, E.; Hess, B.; van der Spoel, D. *J. Mol. Model.* **2001**, *7*, 306−317.
(56) Lee, B.; Richards, F. M. *J. Mol. Biol.* **1971**, *55*, 379−400.
(57) Kabsch, W.; Sander, C. *Biopolymers* **1983**, *22*, 2577−2637.
(58) Ichiye, T.; Karplus, M. *Proteins* **1991**, *11*, 205−217.
(59) Garcia, A. E. *Phys. Rev. Lett.* **1992**, *68*, 2696−2699.
(60) Amadei, A.; Linssen, A. B.; Berendsen, H. J. *Proteins* **1993**, *17*, 412−425.
(61) Hess, B. *Phys. Rev. E* **2000**, *62*, 8438−8448.
(62) Hess, B. *Phys. Rev. E* **2002**, *65*, 031910.
(63) Fogolari, F.; Brigo, A.; Molinari, H. *J. Mol. Recognit.* **2002**, *15*, 377−392.
(64) Sharp, K. A.; Honig, B. *Annu. Rev. Biophys. Biophys. Chem.* **1990**, *19*, 301−332.
(65) Baker, N. A.; Sept, D.; Joseph, S.; Holst, M. J.; McCammon, J. A. *Proc. Natl. Acad. Sci. U.S.A.* **2001**, *98*, 10037−10041.
(66) Notice that using a lower number of water molecules causes a decrease in the calculated unit cell parameters in the NPT MD simulation (see the Supporting Information).
(67) http://people.sissa.it/∼berrera/CAP.html, October 2006.
(68) Olson, W. K.; Gorin, A. A.; Lu, X. J.; Hock, L. M.; Zhurkin, V. B. *Proc. Natl. Acad. Sci. U.S.A.* **1998**, *95*, 11163−11168.
(69) Humphrey, W.; Dalke, A.; Schulten, K. *J. Mol. Graphics* **1996**, *14*, 33−38.
(70) Laaksonen, L. *J. Mol. Graphics* **1992**, *10*, 33−34.
(71) Bergman, D. L.; Laaksonen, L.; Laaksonen, A. *J. Mol. Graphics Modell.* **1997**, *15*, 301−306.
(72) Koradi, R.; Billeter, M.; Wuthrich, K. *J. Mol. Graphics* **1996**, *14*, 51−55.